

# Geophysical Research Letters<sup>®</sup>



## RESEARCH LETTER

10.1029/2023GL103875

### Key Points:

- We develop a method to quantify river planform change after flood events, using Google Earth Engine
- We do so for a data set of 175 floods that exceeded the 80th percentile stage, at 34 flow gauging sites on laterally active rivers
- Planform erosion during these high-flow events was most correlated with the event duration, and then the summed hydrograph

### Supporting Information:

Supporting Information may be found in the online version of this article.

### Correspondence to:

A. S. Leenman,  
[anya.leenman@vuw.ac.nz](mailto:anya.leenman@vuw.ac.nz)




### Citation:

Leenman, A. S., Slater, L. J., Dadson, S. J., Wortmann, M., & Boothroyd, R. (2023). Quantifying the geomorphic effect of floods using satellite observations of river mobility. *Geophysical Research Letters*, 50, e2023GL103875. <https://doi.org/10.1029/2023GL103875>

Received 29 MAR 2023

Accepted 9 AUG 2023

## Quantifying the Geomorphic Effect of Floods Using Satellite Observations of River Mobility

A. S. Leenman<sup>1,2</sup> , L. J. Slater<sup>1</sup> , S. J. Dadson<sup>1,3</sup> , M. Wortmann<sup>1,4</sup>, and R. Boothroyd<sup>5,6</sup> 

<sup>1</sup>School of Geography and the Environment, University of Oxford, Oxford, UK, <sup>2</sup>School of Geography, Environment and Earth Sciences, Te Herenga Waka - Victoria University of Wellington, Wellington, New Zealand, <sup>3</sup>UK Centre for Ecology and Hydrology, Wallingford, UK, <sup>4</sup>European Centre for Medium-Range Weather Forecasts, Reading, UK, <sup>5</sup>School of Geographical and Earth Sciences, University of Glasgow, Glasgow, UK, <sup>6</sup>Now at School of Environmental Sciences, University of Liverpool, Liverpool, UK

**Abstract** Geomorphologists have long debated the relative importance of disturbance magnitude, duration, and frequency in shaping landscapes. For river-channel adjustment by floods, some argue that the cumulative hydrograph, rather than magnitude or duration, matters most. However, studies of flood-induced river-channel change often draw upon small data sets. Here, we combine Sentinel-2 imagery with flow data from laterally active rivers to address this question using a larger data set. We apply automated algorithms in Google Earth Engine to map rivers and detect their lateral shifting; we generate a large data set to quantify planform erosion during 175 floods at 34 selected sites. Erosion during these floods is best explained by their duration and then their cumulative hydrograph. We use a random forest regression model to predict flood-induced erosion, with potential applications for hazard management. Ultimately, better global data on sediment supply and caliber would help us to understand flood-driven change to river planforms.

**Plain Language Summary** Some rivers change their shape over time. In this paper, we explore how high-flow events drive these river channels to reshape themselves. We use Google Earth Engine to automatically map the shapes of rivers in satellite images. We apply this method to pairs of satellite images before and after high-flow events, to understand how the river shape is changed by the event. We compare the amount of channel widening measured to aspects of the high-flow event, including its peak, duration, and total flow. We do so for 175 events, and find that the duration and total flow are most important for explaining how much a channel widens during the event. Finally, we build a statistical model to predict the average amount of channel widening for a given high-flow event. This method has potential applications for hazard management in rivers that are known to change their shape.

## 1. Introduction

The relative importance of disturbance magnitude, duration, and frequency for shaping landscapes is a crucial question in geomorphology. Many studies have considered the effects of high-magnitude versus high-frequency events: for cumulative sediment transport (Webb & Walling, 1982; Wolman & Miller, 1960), for generating and reworking landforms (Kale, 2002, 2003; Surian et al., 2015; Wolman & Gerson, 1978), and for the resulting sedimentology (Magilligan et al., 1998; Marren, 2005). Others have considered the duration and total energy expenditure of individual disturbances and how this relates to their ability to transport sediment and reshape river channels (Costa & O'Connor, 1995; Magilligan et al., 2015; Rose et al., 2020). In rivers, understanding which disturbances perform the most geomorphic work—both instantaneously, and cumulatively over time—has important implications for sediment budgeting, flood conveyance, depositional records, and natural hazard management.

In rivers, the major disturbances are flood events, which have the power to reshape the channels that convey them. Observed flood reshaping ranges from bar deposition and bank erosion (Bryndal et al., 2017), incision (Gibson & Shelley, 2020; Hajdukiewicz et al., 2016), or aggradation (Hooke, 2016; Morche et al., 2007) through to widening (Fuller, 2008; Hajdukiewicz et al., 2016; Yousefi et al., 2018), reoccupation of abandoned channels (Arnaud-Fassetta et al., 2005) and large-scale reworking of floodplains (Miller, 1990). The latter can have severe societal impacts, including erosion of agricultural or residential land (Yousefi et al., 2018) or the destruction of transport and river management infrastructure (Arnaud-Fassetta et al., 2005). Conversely, aggradation during

© 2023. The Authors.

This is an open access article under the terms of the [Creative Commons Attribution License](https://creativecommons.org/licenses/by/4.0/), which permits use, distribution and reproduction in any medium, provided the original work is properly cited.

floods can raise riverbeds by several meters (Morche et al., 2007; Tunncliffe et al., 2018), reducing a channel's conveyance capacity and the freeboard below bridges (Johnson et al., 2001). Quantitative methods are needed to understand, model, and predict how river channels can be reshaped by individual flood events.

The geomorphic effectiveness of a flood is thought to be a function of its duration and magnitude. Here, we define geomorphic effectiveness as the extent to which a flood alters the channel form by eroding or depositing sediment. We use the term “flood” to mean any temporary rise in the water level (in our analysis, one that exceeds the 80th percentile of the water surface elevation measurements). Previous studies have suggested that the cumulative stream power (defined by Bagnold (1966) as the product of water density, acceleration due to gravity, discharge and slope) beneath a flood hydrograph must be high for the event to be geomorphically effective; the implication is that high-magnitude but brief floods, and low-magnitude but long floods, are not likely to be effective (Costa & O'Connor, 1995). However, others have suggested that additional factors (not just the cumulative power) make a flood geomorphically effective. For instance, Middleton et al. (2019) demonstrated that flood magnitude does influence geomorphic effectiveness: in the proglacial braided river they studied, planform change during floods increased with their peak discharges. Others propose that a flood's geomorphic effectiveness is not determined by its hydrograph alone, but also by its sediment supply (Arkesteijn et al., 2019; Bennett et al., 2017; Church et al., 2014; Hooke, 2016; Pfeiffer et al., 2019) or the time since the previous flood, which can influence both sediment availability and the looseness of the riverbed (Gintz et al., 1996; Hooke, 2015). These studies have advanced our understanding of geomorphic effectiveness, but almost all were small-sample case studies of 1–10 flood events or river reaches, often in similar environmental contexts. Larger samples of flood events from a more geomorphically diverse set of rivers are required to produce a robust empirical assessment of what makes a geomorphically effective flood.

Google Earth Engine (GEE) has recently emerged as a key tool facilitating large-sample analyses of landscape characteristics—through both its computational platform and archive of quality-controlled satellite data. The “large-sample” approach, which addresses environmental questions using data from tens to thousands of sites, is popular in hydrology (Addor et al., 2017; Klingler et al., 2021) and has begun to be applied in geomorphology (Ahrendt et al., 2022; Brooke et al., 2022; Clubb et al., 2022; Edmonds et al., 2022; Pfeiffer et al., 2019; Slater, 2016; Slater et al., 2015; Sylvester et al., 2019; Valenza et al., 2020). A large-sample approach to studying planimetric river change can be readily deployed in GEE, drawing on automated methods to map river planform (Allen & Pavelsky, 2015; Boothroyd et al., 2021; Isikdogan et al., 2019; Pekel et al., 2016; Pickens et al., 2020; Zou et al., 2018) and to track planform deformation (Chadwick et al., 2022; Jarriel et al., 2021; Langhorst & Pavelsky, 2022; Rowland et al., 2016; Schwenk et al., 2017; Wickert et al., 2013). By automating river planform tracking in GEE, the geomorphic effectiveness of a large sample of flood events can be assessed.

In this paper, we investigate the streamflow drivers of geomorphically effective floods using Sentinel-2 satellite imagery in GEE. We pursue two research questions:

1. Which hydrograph metrics best explain a flood's geomorphic effectiveness?
2. How well can a flood's geomorphic effectiveness be predicted from hydrologic variables?

Because of the 2D nature of satellite data, we measure geomorphic effectiveness as the planform erosion caused by a flood. We compute this erosion in GEE for flood events in Brazil, Colombia, New Zealand and Russia. We use 175 events at 34 flow gauging sites on laterally active rivers to evaluate our research questions (see Figure S1 in Supporting Information S1, for gauge locations). We ascertain the influence of hydrograph shape on planform erosion in our data set. Finally, we develop an empirical model to predict flood-induced erosion. When coupled with streamflow forecasts, the model may be useful for hazard management in sites that are known to be laterally active.

## 2. Methods

Our method has four steps: (a) site selection and area of interest generation, (b) flood delineation and search window definition, (c) planform extraction and change detection, and (d) regression and prediction. These steps are detailed below, and summarized in Figure 1. Our code is available at <https://github.com/a-leenman/2dFloodsPublic>; GEE processing was performed via the “rgee” r package (Aybar, 2022).

### 2.1. Site Selection and Area of Interest

Hydrologic records are crucial to our analysis, providing flood occurrence and hydrograph shape data. We obtained publicly available stage records and gauging locations for Brazil, Colombia, New Zealand, and Russia. These countries were chosen for their laterally active rivers and availability of daily stage records.

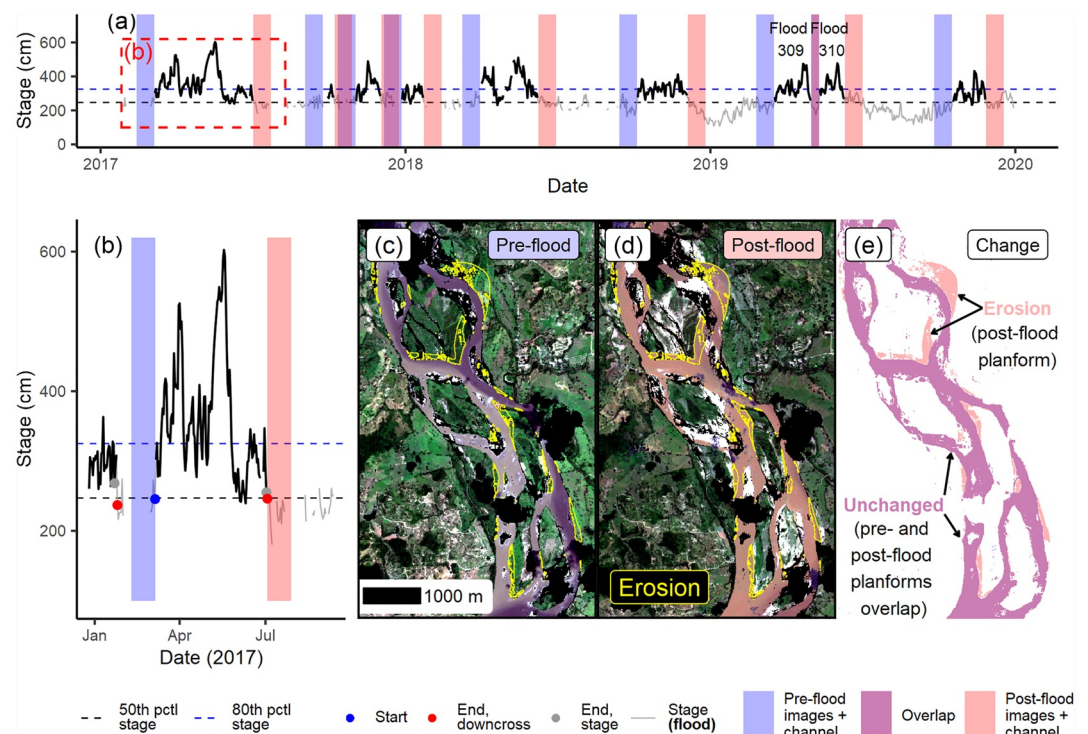


**Figure 1.** Methods to define floods and detect planform change. (a) The pre-flood (blue) and post-flood (pink) search windows for a sequence of floods (bold lines); windows can overlap (purple). (b) Example flood from Colombian gauge 23097040, with the flood start date (blue circle), two options for flood end date (gray and red circles) and the pre- and post-flood search windows. (c) Pre-flood channel morphology, mosaicked from all cloud-free pixels in the six satellite images covering the Area of Interest within the pre-flood search window. Planform erosion during the following flood is outlined in yellow. Black patches have no data due to cloud. (d) Corresponding post-flood mosaic (10 images within the time and space filter). (e) The pre- and post-flood channels are overlaid, highlighting the planform erosion.

Other authors used discharge or stream power records to pursue this problem. However, we chose to use stage data so that differences in stage could provide a proxy for depth fluctuations when estimating shear stress and sediment transport capacity.

We filtered the stage records to include only those gauges that:

1. Were located on a river with a mean annual discharge above  $100 \text{ cm}^3 \text{ s}^{-1}$  (data from Grill et al. (2019)) and width above 150 m, to ensure these rivers were large enough to be visible in our 10 m satellite imagery.
2. Were located on a laterally active river whose dynamics could be measured from satellite data. Laterally active rivers were identified by filtering the “water permanence” layer from Pekel et al. (2016). After computing planform change during floods, a site was removed if the eroded area never exceeded 1% of the water surface area and if reach-averaged widening never exceeded 5 m. These thresholds enabled the largest possible data set while excluding channels that were not laterally active.
3. Were not adjacent to large lakes or dams.
4. Overlapped with the Sentinel-2 record (June 2015–present) by at least one year.

This filtering isolated a sample of 34 gauges. Observed river widths ranged from 150 to 1,600 m; gradients (extracted along each reach from the Yamazaki et al. (2017) DEM) ranged from 0.00001 to 0.003. Estimated mean long-term discharges ranged from 110 to  $7,300 \text{ cm}^3 \text{ s}^{-1}$ , and upstream catchment area ranged from 1,400 to 430,000  $\text{km}^2$  (Grill et al., 2019). Richards-Baker indices (Baker et al., 2004) ranged from 0.005 (very seasonal) to 0.33 (moderately flashy). Gauge altitudes ranged from 15 to 600 m, local forest cover from 0% to 90%, and mean annual precipitation from 400 to 4,000 mm (Linke et al., 2019). The range of rivers (including braided, wandering and meandering forms) encompassed by these values highlights the geographic and geomorphic diversity of the rivers we incorporate, summarized in Figures S2 and S3 in Supporting Information S1.

For each gauge, we defined an “Area of Interest” (AOI) within which we extract the river planform and monitor its deformation. The “HydroSHEDS Free Flowing Rivers” vector network (Grill et al., 2019; Lehner et al., 2008) was used to select all river segments within 40 km of each gauge. We kept only the segments on the same branch as the gauge, and also removed segments that were past a jump in average discharge of >20%, implying that a “major” tributary had been passed; we computed such jumps using the average discharge data for each segment in Grill et al. (2019). If two gauges were nearby on the same river, we divided the intervening segments between them. This left a “linked reach” (comprising one or more HydroSHEDS segments) assigned to each gauge. We extracted water masks along each reach from Allen and Pavelsky (2018a, 2018b), as a first approximation of the channel area. However, these masks do not always encompass the entire channel in our study reaches (which are extremely laterally mobile: some shift by over 30 m in a single flood) and so we buffered these masks by 500 m to create the AOI. Finally, lakes in the HydroLAKES (Messager et al., 2016) data set were subtracted from the AOI, to avoid spurious change detection from varying lake levels. We thus assigned to each gauge a unique AOI within which we extracted the river planform before and after each flood.

## 2.2. Flood Delineation and Search Window Definition

We delineated floods temporally based on the daily stage record for each gauge. Although higher frequency records were available for some countries, we resampled them by taking the daily mean stage. While this process smoothed some maxima and minima, it gave all records the same frequency. We defined a flood as any period exceeding the 80th percentile of the stage record during the Sentinel-2 record (June 2015 onwards; Figures 1a and 1b). Floods were extracted using the hydroEvents R package (Wasko & Guo, 2022). To ensure we captured the rising and falling limbs, we defined the flood start date as the first pre-peak measurement below the 50th percentile of stage (Figure 1a, blue points). We defined the flood end date in two ways: either as

1. the first post-peak measurement below the 50th percentile of stage (Figure 1a, red points), or
2. the first post-peak measurement within 30 cm of the stage at the start of the flood (Figure 1a, gray points). Occasionally, missing data meant the first method created flood end dates that were unreasonably far after the end of the flood, necessitating the second method.

For each flood, we chose the earliest end date option. Following the discussion in Slater et al. (2021), floods separated by less than 7 days were counted as one event, and floods longer than 5 months were discounted as these were mostly anomalies from missing data. While using the 50th percentile to give the start and end dates assigns a longer length to floods than some approaches, it allows us to capture the geomorphic effects of the rising and falling limbs, and recognizes that geomorphic change and sediment entrainment could start before the 80th percentile stage is exceeded.

Directly before and after each flood, we defined pre- and post-flood time windows of up to 25 days (Figures 1a and 1b). We truncated a time window if floods were less than 25 days apart; for example, flood 309 (Figure 1a) finished nine days before the following event, and so its post-flood window was truncated. If sequential events were less than 50 days apart, their pre- and post-flood windows could overlap; the post-flood window for one flood could even overlap entirely with the pre-flood window of the following event, as with floods 309 and 310 (Figure 1a; this meant the post-flood channel mask of flood 309 was reused as the pre-flood mask of flood 310). We used these pre- and post-flood time windows to search the Sentinel-2 archive (Level 1C, harmonized; Copernicus, n.d.).

## 2.3. Planform Extraction and Change Detection

Within each pre- and post-flood time window, we extracted the river planform from Sentinel-2 (S2) imagery. First, we mosaicked all cloud-free S2 pixels within the time window and AOI, taking the minimum reflectance in each band if multiple copies of one pixel were available. Figures 1c and 1d are examples of these mosaics. We proceeded with an event if at least 50% of its AOI was cloud-free; only pixels that were cloud-free in both mosaics were used. For sites in New Zealand and Russia, we also mapped snow using the normalized difference snow index, following Hofmeister et al. (2022). For snow-free scenes that met our cloud threshold, we mapped channel planform using the methods of Zou et al. (2018) and Boothroyd et al. (2021), who mapped water by combining the normalized difference vegetation index (Rousel et al., 1973), modified normalized difference water index (Xu, 2006), and enhanced vegetation index (Huete et al., 2002). Clumps of “channel” smaller than



10 pixels were removed. Following Boothroyd et al. (2021), we counted both water and exposed sediment (i.e., non-vegetated bars) as part of the channel, given that a lack of vegetation indicates bars are frequently inundated. This mapping method is simple but generalizable to rivers with different lighting conditions and suspended sediment concentrations.

We conducted change detection between the pre- and post-flood planforms to estimate each flood's geomorphic effectiveness. To isolate areas that were permanently (as opposed to transiently) changed during a flood, we tracked the state (wet or dry) of each pixel at monthly intervals for the following 24 months, loosely following the pixel-by-pixel trend analysis of Nagel et al. (2022). We only considered a pixel to be eroded if it switched from dry-to-wet in the flood and then continued to be wet for the subsequent 2 years. If cloud cover meant there were <18 months of these after-flood observations for an event, we discounted it; we chose this threshold by checking the change detection for bias due to stage fluctuations. This pixel-tracking method allowed us to eliminate spurious change detection resulting from transient stage fluctuations.

We measured a flood's geomorphic effectiveness as the planform area that was eroded (i.e., permanently changed from “dry” to “wet”) during the event. We normalized the eroded area by water surface area (accounting for differences in river width across our sites, as channel size can positively influence channel mobility (Constantine et al., 2014; Langhorst & Pavelsky, 2022; Nanson & Hickin, 1986)) to give “normalized planform erosion” (NPE). Because we counted non-vegetated bars as part of the channel, it was difficult to measure deposition following the flood; newly deposited sediment was typically registered as “channel” by our mapping algorithm. This is why we consider post-flood erosion of the vegetated channel boundary (i.e., NPE) to be the most appropriate metric of geomorphic effectiveness in this data set.

Our procedures for gauge selection, cloud- and snow-filtering isolated a data set of 175 events for which we measured NPE. Because there were only 11 floods observed in some countries, we pooled all events for our subsequent analyses.

#### 2.4. Regression and Prediction

Our first research question considers the influence of hydrograph shape on geomorphic effectiveness. There are numerous metrics to characterize hydrographs, including measures of height, duration, integrated power, volume or transport capacity, and asymmetry (Brunner et al., 2021; Slater et al., 2021). Because these rivers feature a range of hydrographs (for instance, flashy vs. seasonal), we use three simple metrics that allow comparison with previous studies. The first is the flood peak height, relative to the mean daily stage. The second is the cumulative value of all daily stage measurements during the flood, measured relative to mean daily stage. This cumulative water level metric is akin to the “volume” of a hydrograph when using discharge records (e.g., Brunner et al., 2021, Figure 3). Because we use stage records, the metric accounts for the combined influence of changes in flow depth during the flood (exerting stress on the river banks/bed) and of flood duration; we refer to it as the “summed hydrograph.” The third metric is the flood duration.

As well as exploring how hydrograph metrics correlated with NPE, we built a random forest (RF) regression model to rank these metrics' importance (by estimating how much they decreased the model's mean square error [MSE]). Although sediment supply increases channel mobility (e.g., Ahmed et al., 2019; Constantine et al., 2014; Donovan et al., 2021), we do not have sediment supply time-series for our gauging sites. Instead, we used stream gradients and stage records to estimate the sediment transport capacity for each flood (see Section S1 in Supporting Information S1 for details), and added these estimates to the RF model; all predictors are listed in Table S2 in Supporting Information S1. We built the model using the randomForest r package (Liaw & Wiener, 2002) and combined it with leave-one-out cross-validation (LOOCV) to predict each flood's NPE. Details on the RF model and LOOCV are in Section S1 in Supporting Information S1.

### 3. Results

In the laterally active rivers we study, floods and their geomorphic effectiveness vary by orders of magnitude (Figure 2). Peak heights vary from 30 to 800 cm above mean daily stage. The summed hydrographs vary from 40 to 30,000 cm above mean daily stage, and flood durations from 3 to 150 days. The geomorphic effectiveness of these floods is diverse, with planform erosion as low as 0.006% of the total water surface and as high as 7.6%,

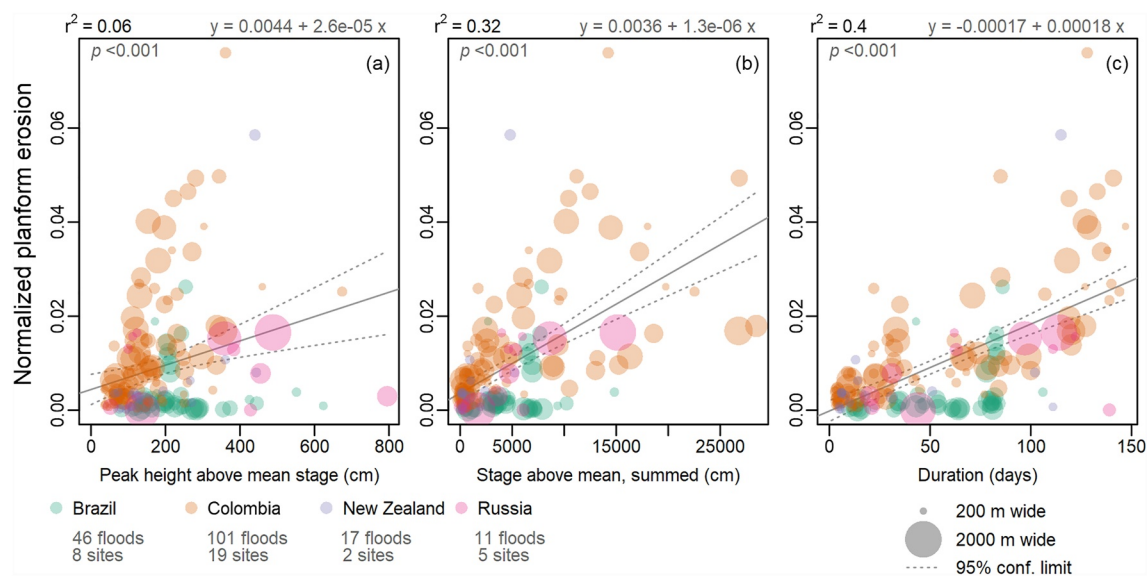


**Figure 2.** Flood metrics and their relationship to normalized planform erosion during each flood. (a) Flood peak height above the mean daily stage. (b) Cumulative stage exceeding mean daily stage (“summed hydrograph”). (c) Flood duration. Each point represents one event; colors indicate the four countries; point size is proportional to pre-flood channel width. The solid gray line shows a linear regression and dotted lines show 95% confidence limits; the regression equation is at the top-right.  $r^2$  and  $p$ -values are at the top left.  $r^2$  values for individual countries are in Table S1 in Supporting Information S1.

with absolute reach-averaged widening up to 42 m. The most active country our data set is Colombia, with an average NPE of 1.2% across all floods.

Our first research question considers the erosional response of river channels to flood hydrographs. Figure 2 demonstrates how NPE varies with three hydrograph metrics in the 175 floods we study. Each point represents one event, with the NPE compared to the flood's peak height (a), summed hydrograph (b), and flood duration (c). Figure 2 therefore shows how hydrograph metrics influence geomorphic effectiveness for 175 floods at 34 sites across Brazil, Colombia, New Zealand, and Russia between 2015 and 2021.

Our results indicate that NPE is unrelated to flood height in our data set (Figure 2a). A linear regression of NPE against flood peak height had an  $r^2$  of just 0.06. Erosion scaled more strongly with the summed hydrograph (Figure 2b), with an  $r^2$  of 0.32, and most strongly with flood duration (Figure 2c), with an  $r^2$  of 0.40. See Table S1 in Supporting Information S1 for country-specific relationships. These coefficients of determination are surprisingly high, considering that they represent observations from real systems and are thus confounded by other natural variables in each location. Some of the relationships in Figure 2 appear non-linear, but we lack sufficient data to fit non-linear models and so use linear regression for a first-order comparison. These metrics are correlated among themselves (see Figure S8 in Supporting Information S1); longer floods often had higher peaks, so that the  $r^2$  values shown here indicate *relative* importance and we cannot say that the increase in erosion with flood duration was independent of the concurrent increase in height for many floods. Nevertheless, panels (a–c) indicate that, at least for our sample of laterally active rivers, flood duration was the most important variable for explaining flood-driven erosion of the vegetated channel boundary.

We built a RF regression model to rank the importance of the hydrograph metrics and estimated sediment transport for explaining NPE. The RF model ranked these variables in the following order: estimated transport, flood duration, summed hydrograph, and peak height; the rankings reflect how much each variable reduced the model's MSE. This ranking is similar to the  $r^2$  values in Figure 2 and Figure S9 in Supporting Information S1. Because the summed hydrograph and flood duration were correlated ( $R = 0.82$ ), we ran two additional model versions, omitting either summed hydrograph or flood duration. Although these omissions altered the variables' MSE reductions, neither altered the remaining variable rankings, implying that the rankings are not affected by this co-linearity in the predictors.

We predicted NPE for all floods in our data set using the RF model with LOOCV. We were able to predict NPE with at least 55% accuracy ( $R = 0.74$ ; Figure 3c) using the pooled data set. The model performed best for sites in

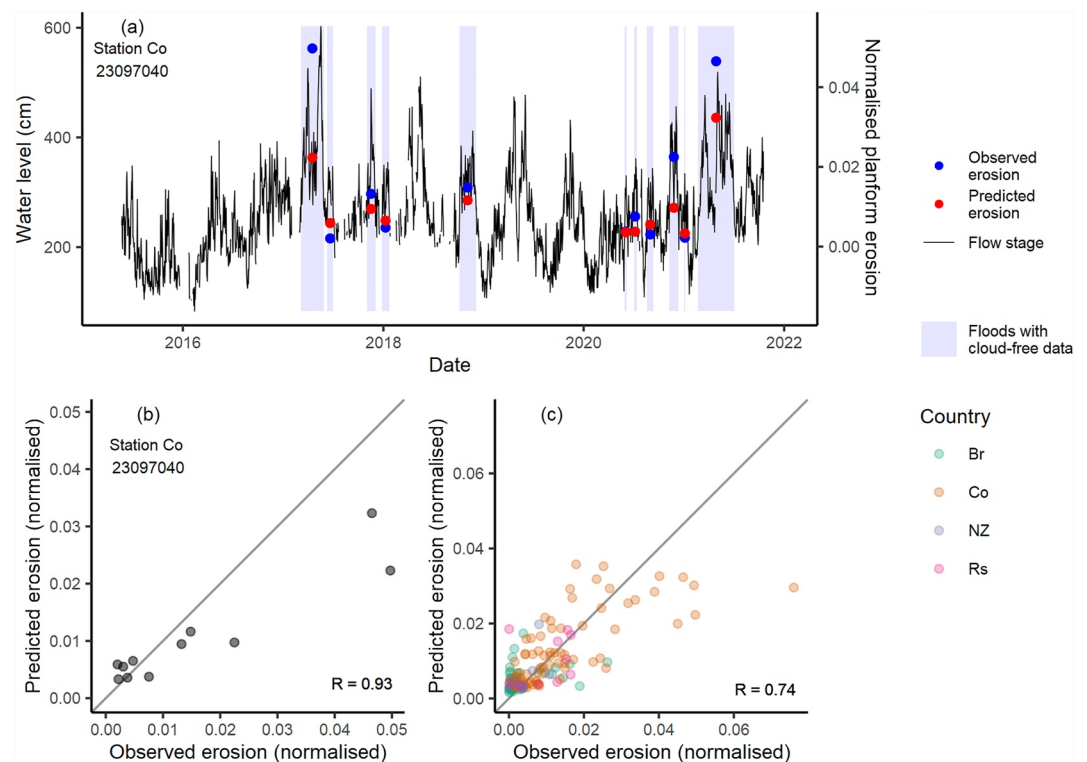


**Figure 3.** Predictions from our random forest regression model. (a) The stage record for Colombian gauge 23097040; flood events with sufficient cloud-free satellite data are highlighted. The observed and predicted normalized platform erosion (NPE) during each flood are overlain and scale with the secondary y-axis. (b) A comparison of observed and predicted NPE at this gauge; each point is one flood. (c) A comparison of observed and predicted NPE for all floods in our data set. Gray lines in panels (b, c) show a 1:1 relation.

Colombia with numerous floods, such as site 23097040 (Figures 3a and 3b). For Colombian sites with data for  $>7$  floods,  $R$  values were 0.62–0.96. The model tended to under-predict the highest values of reach-averaged erosion, which reflects our choice of model—RF models do not predict outside their training data range.

#### 4. Discussion

Although there is no firm consensus, previous literature has laid the case for a hydrograph's cumulative power as the best explainer of a flood's geomorphic effectiveness. For instance, based on 10 events in Arkansas, California, Colorado, Idaho, Oregon, and Washington, Costa and O'Connor (1995) suggested that a flood's geomorphic effectiveness reflected the cumulative unit stream power exceeding the threshold for alluvial erosion. Rose et al. (2020) likewise found that the most geomorphically effective floods in a sample of seven had a high energy expenditure, high peak and long duration. Kale and Hire (2007) observed that sediment transport (a proxy for geomorphic effectiveness) during monsoons rose exponentially with their cumulative power. Magilligan et al. (2015) attributed the limited widening during an extreme flood to its low cumulative power, resulting from a high peak but short duration. Our data partly support this hypothesis; the summed hydrograph was positively correlated with planform erosion during the floods we studied. However, in our data set flood duration was a better predictor of erosion of the vegetated channel boundary. This result was consistent when we altered the flood definition threshold to the 70th or 90th percentile of stage (Figures S10 and S11 in Supporting Information S1).

One reason for the weaker influence of the summed hydrograph in our data may be that these previous studies used the unit stream power hydrograph, whereas we used the stage hydrograph. We used stage so that changes could be used as a proxy for depth fluctuations when estimating shear stress and sediment transport capacity. Another reason for the weak influence of the summed hydrograph in our large-sample analysis may be our inability to ascertain the threshold of motion for every flood at every site in our data set; we had no data on grain size distributions, bed structure, and their spatio-temporal variability. Conversely, other studies measured hydrographs

relative to an erosion threshold that they were able to determine from in-depth analysis of a small data set (e.g., Rose et al., 2020).

The importance of flood duration in our data set implies that, once these floods exceed the entrainment threshold, further stage increases have a smaller effect than the duration above that threshold. That is, the duration of above-threshold shear stress has a greater effect than the peak stress. This result implies that the threshold for entrainment was low in the rivers we studied, so that full mobility of all sediment sizes was attained frequently. The regional breakdown of Figure 2 (Table S1 in Supporting Information S1) supports this notion, as the influence of duration is strongest for Colombia where others have reported sand beds (e.g., Martínez Silva & Nanny, 2020; Smith, 1986). Table S1 in Supporting Information S1 also highlights the influence of the Colombian data set (101 of 175 floods) on our results; offsetting this influence was a motivation for pooling our data.

Other studies have used flood peak height, rather than cumulative hydrographs, to explain geomorphic effectiveness. For instance, Middleton et al. (2019) mapped planimetric change during floods in a proglacial river and showed that, once a threshold discharge had been exceeded, planimetric change increased with peak discharge. Miller (1990) found that, in alluvial rivers wider than 200 m, peak unit stream power during floods was correlated with geomorphic effectiveness. In alluvial fan experiments featuring different hydrographs of the same volume, surface reworking volumes increased with the peak discharge (Leenman et al., 2022). Nevertheless, in our data set flood height was not related to NPE. It is possible that a threshold above which peak height becomes important can only be extracted by analyzing numerous floods at one location. Such an analysis is difficult in the remote sensing of real rivers, either due to infrequent floods or to persistent cloud cover, both of which limit the number of events that can be assessed.

Our results highlight some complexities of investigating flood impacts with a large-sample remote-sensing analysis. First, while we measured the flood-induced erosion of the vegetated channel boundaries, others categorized flood effects qualitatively (e.g., Costa & O'Connor, 1995) or quantified sedimentological impacts (Magilligan et al., 2015). The importance of duration here is relevant to vegetated channel boundaries, but results may differ if measuring a different aspect of channel morphology—for instance, Magilligan et al. (2015) highlight how a flood event can have large sedimentological effects (for instance, depositing coarse material on floodplains) but a smaller impact on channel shape. Second, our large-sample analysis highlights the difficulty of finding a single parameter explaining geomorphic effectiveness in all rivers. Flood duration was the most important driver of erosion in some rivers in our data set, but not all; Table S1 in Supporting Information S1 shows that peak height was more important in Russia and New Zealand. Third, the relationship between a flood hydrograph and the erosion caused can be compounded by other variables, including the presence and character of vegetation, the caliber and structure of bed and bank sediment, the sediment supplied from upstream, the channel geometry, and the time elapsed since the previous flood. In this paper, we make a first attempt at a large-sample analysis of geomorphically effective floods, and our work highlights the need for global data sets on these additional variables in order to fully address this problem.

Others have suggested that the causal relationship between a flood and its geomorphic effectiveness is moderated by sediment supply. For instance, in comparing two events on the Peace River (Canada), Church et al. (2014) found that their geomorphic effects were best explained by differences in the sediment influx. Pfeiffer et al. (2019) found that bed-level changes in Washington State were not related to high-flow events, but to sediment supply from glaciers upstream. Dean and Schmidt (2013) observed that geomorphic change during a flood in the Rio Grande was highest downstream of sediment-rich tributaries. For longer-term channel mobility, sediment supply positively influences channel migration (Constantine et al., 2014), and some rivers in our data set (e.g., the Magdalena) have very high sediment loads (Dethier et al., 2022; Higgins et al., 2016; Restrepo et al., 2006). This question is an interesting and important one, and further work to measure sediment transport alongside flow during floods is crucial for understanding how sediment availability modulates a hydrograph's geomorphic effectiveness.

Our methods have some limitations which provide avenues for further research. The first is the suitability of using planform measurements to quantify three-dimensional channel adjustment. For landslides, erosional area scales with volume (Guzzetti et al., 2009; Larsen et al., 2010), but in rivers a 2D for 3D substitution would not be appropriate where channels are laterally confined. We have side-stepped this problem by using only laterally mobile rivers, which are therefore the rivers where a 2D for 3D substitution is most appropriate. Middleton et al. (2019) demonstrated experimentally that sediment transport scaled linearly with planimetric change, providing further



justification for 2D change detection. However, further research on the suitability of measuring geomorphic effectiveness in planview would be valuable.

Further potential limitations include that of data resolution; the Sentinel-2 imagery we use has a 10 m resolution. Because erosion may occupy a smaller footprint than deposition of the same volume (Lindsay & Ashmore, 2002), finer-scale imagery may better capture erosion and would facilitate equal monitoring of both processes. An investigation of improvements with higher-resolution imagery would be worthwhile. In addition, our method computes change in the vegetated channel boundaries, so that non-vegetated bars moving through these rivers are not counted. Work comparing different algorithms to quantify river dynamics would be a useful contribution. Finally, similarity between the spectral signatures of snow and water in the mNDWI (Huang et al., 2018) meant we had to discard snowy scenes. We thus compromised slightly on our goal of a geomorphically diverse set of rivers. As the S2 record approaches a decade, the main limitation on this work is the availability of flow records, which constrains the range of sites that can be used. Methods to measure or model flow in ungauged basins could extend this work to an even more geographically diverse range of rivers.

## 5. Conclusions

We used GEE and the Sentinel-2 satellite archive to map planform erosion in laterally mobile rivers during 175 flood events. By tracking each pixel for 2 years, we were able to separate erosion from transient water extent fluctuations arising from stage variability. We measured each flood's geomorphic effectiveness as the flood-induced planform erosion (normalized by water surface area), and compared this to the flood hydrograph.

In the 34 laterally active rivers studied, we found that the flood peak height was not correlated with erosion. The summed hydrograph was a better predictor, but erosion correlated most strongly with flood duration in our data set of events exceeding the 80th percentile of stage.

We built a RF regression model to predict planform erosion for each flood, using hydrograph metrics and estimated sediment transport. The model had a prediction accuracy of 55%, which is promising for forecasting flood-driven riverbank erosion in laterally active reaches.

Our work highlights the need for high-frequency flow monitoring in the world's laterally active rivers, to better understand how a flood's hydrograph controls its erosional impact. Moreover, better data on land cover, bank strength, and sediment caliber at stream gauging sites would elucidate how these characteristics modulate flood-driven erosion. Finally, monitoring sediment transport alongside river flows would help us to understand how sediment availability influences a flood's geomorphic effectiveness.

## Data Availability Statement

The code used to quantify erosion during each flood event is available at <https://github.com/a-leenman/2dFloodsPublic>. We have uploaded the data underlying our figures to <https://zenodo.org/record/8170280>. The stage records used were accessed via the following links:

- Brazil: downloaded from ANA (Agência Nacional de Águas) via <http://www.snirh.gov.br/hidroweb/apresentacao>.
- Colombia: downloaded from IDEAM (Instituto de Hidrología, Meteorología y Estudios Ambientales) via <http://dhime.ideam.gov.co/atencionciudadano/>.
- New Zealand: downloaded from NIWA (National Institute of Water and Atmospheric Research)/Taihoro Nukurangi via <https://hydrowebportal.niwa.co.nz/Data/DataSet/Export/Location/68526/DataSet/Stage/Master/Interval/Yearly/Calendar/CALENDARYEAR/2018> (Station ID can be selected at top).
- Russia: downloaded from the Federal Agency for Water Resources (<https://voda.gov.ru/otkrytoe-agentstvo/opendata/>). The data were accessed via <https://gis.favr.ru/web/guest/opendata>, although this link was broken at the time of writing.

## Acknowledgments

We would like to thank the editor, one anonymous reviewer, and Clàudia Ylla Arbós for their thoughtful and constructive reviews which improved the quality of our work. We would also like to thank Dr. Yinxue Liu for her assistance in sourcing flow data. We are grateful to the numerous colleagues who discussed the work with us and provided feedback. ASL would like to thank Christ Church college, Oxford for their support and hospitality during her JRF. LJS is supported by UKRI (MR/V022008/1 and NE/S015728/1).

## References

- Addor, N., Newman, A. J., Mizukami, N., & Clark, M. P. (2017). The CAMELS data set: Catchment attributes and meteorology for large-sample studies. *Hydrology and Earth System Sciences*, 21(10), 5293–5313. <https://doi.org/10.5194/hess-21-5293-2017>
- Ahmed, J., Constantine, J. A., & Dunne, T. (2019). The role of sediment supply in the adjustment of channel sinuosity across the Amazon Basin. *Geology*, 47(9), 807–810. <https://doi.org/10.1130/g46319.1>
- Ahrendt, S., Horner-Devine, A. R., Collins, B. D., Morgan, J. A., & Istanbuluoglu, E. (2022). Channel conveyance variability can influence flood risk as much as streamflow variability in western Washington state. *Water Resources Research*, 58(6), e2021WR031890. <https://doi.org/10.1029/2021wr031890>
- Allen, G. H., & Pavelsky, T. M. (2015). Patterns of river width and surface area revealed by the satellite-derived North American River width data set. *Geophysical Research Letters*, 42(2), 395–402. <https://doi.org/10.1002/2014gl062764>
- Allen, G. H., & Pavelsky, T. M. (2018a). Global extent of rivers and streams. *Science*, 361(6402), 585–588. <https://doi.org/10.1126/science.aat0636>
- Allen, G. H., & Pavelsky, T. M. (2018b). Global River widths from landsat (GRWL) database [Dataset]. Zenodo. <https://doi.org/10.5281/ZENODO.1297434>
- Arkesteijn, L., Blom, A., Czapiga, M. J., Chavarrías, V., & Labeur, R. J. (2019). The quasi-equilibrium longitudinal profile in backwater reaches of the engineered alluvial river: A space-marching method. *Journal of Geophysical Research: Earth Surface*, 124(11), 2542–2560. <https://doi.org/10.1029/2019JF005195>
- Arnaud-Fassetta, G., Cossart, E., & Fort, M. (2005). Hydro-geomorphic hazards and impact of man-made structures during the catastrophic flood of June 2000 in the Upper Guil catchment (Queyras, Southern French Alps). *Geomorphology*, 66(1–4), 41–67. <https://doi.org/10.1016/j.geomorph.2004.03.014>
- Aybar, C. (2022). rgee: R bindings for calling the “Earth engine” API [Computer software]. Retrieved from <https://github.com/r-spatial/rgee/>
- Bagnold, R. A. (1966). An approach to the sediment transport problem from general physics (Report No. 4221). <https://doi.org/10.3133/pp4221>
- Baker, D. B., Richards, R. P., Loftus, T. T., & Kramer, J. W. (2004). A new flashiness index: Characteristics and applications to midwestern rivers and streams. *JAWRA Journal of the American Water Resources Association*, 40(2), 503–522. <https://doi.org/10.1111/j.1752-1688.2004.tb01046.x>
- Bennett, G., Kean, J., Rengers, F., Ryan, S., & Rathburn, S. (2017). Landslide-channel feedbacks amplify flood response and channel erosion. In *EGU general assembly conference abstracts*. (p. 14326).
- Boothroyd, R. J., Williams, R. D., Hoey, T. B., Barrett, B., & Prasoj, O. A. (2021). Applications of Google Earth Engine in fluvial geomorphology for detecting river channel change. *Wiley Interdisciplinary Reviews: Water*, 8(1), e21496. <https://doi.org/10.1002/wat2.1496>
- Brooke, S., Chadwick, A. J., Silvestre, J., Lamb, M. P., Edmonds, D. A., & Ganti, V. (2022). Where rivers jump course. *Science*, 376(6596), 987–990. <https://doi.org/10.1126/science.abm1215>
- Brunner, M. I., Slater, L., Tallaksen, L. M., & Clark, M. (2021). Challenges in modeling and predicting floods and droughts: A review. *WIREs Water*, 8(3), e1520. <https://doi.org/10.1002/wat2.1520>
- Bryndal, T., Franczak, P., Krocak, R., Cabaj, W., & Kołodziej, A. (2017). The impact of extreme rainfall and flash floods on the flood risk management process and geomorphological changes in small Carpathian catchments: A case study of the Kasiniczanka river (Outer Carpathians, Poland). *Natural Hazards*, 88(1), 95–120. <https://doi.org/10.1007/s11069-017-2858-7>
- Chadwick, A., Steel, E., Williams-Schaetzel, R., Passalacqua, P., & Paola, C. (2022). Channel migration in experimental river networks mapped by particle image velocimetry. *Journal of Geophysical Research: Earth Surface*, 127(1), e2021JF006300. <https://doi.org/10.1029/2021jfo06300>
- Church, M., Ayles, C. P., & Eaton, B. C. (2014). The floods of 1990 and 1996 on Peace River. In M. Church (Ed.), *The regulation of Peace River* (pp. 233–249). John Wiley & Sons, Ltd. <https://doi.org/10.1002/9781118906170.ch10>
- Clubb, F. J., Weir, E. F., & Mudd, S. M. (2022). Continuous measurements of valley floor width in mountainous landscapes. *Earth Surface Dynamics*, 10(3), 437–456. <https://doi.org/10.5194/esurf-10-437-2022>
- Constantine, J. A., Dunne, T., Ahmed, J., Legleiter, C., & Lazarus, E. D. (2014). Sediment supply as a driver of river meandering and floodplain evolution in the Amazon Basin. *Nature Geoscience*, 7(12), 899–903. <https://doi.org/10.1038/ngeo2282>
- Copernicus. (n.d.). Harmonized Sentinel-2 MSI: MultiSpectral Instrument, level-1C. Retrieved from [https://developers.google.com/earth-engine/datasets/catalog/COPERNICUS\\_S2\\_HARMONIZED#description](https://developers.google.com/earth-engine/datasets/catalog/COPERNICUS_S2_HARMONIZED#description)
- Costa, J. E., & O'Connor, J. E. (1995). Geomorphically effective floods. *Natural and Anthropogenic Influences in Fluvial Geomorphology: AGU Geophysical Monograph*, 89, 45–56.
- Dean, D. J., & Schmidt, J. C. (2013). The geomorphic effectiveness of a large flood on the Rio Grande in the Big Bend region: Insights on geomorphic controls and post-flood geomorphic response. *Geomorphology*, 201, 183–198. <https://doi.org/10.1016/j.geomorph.2013.06.020>
- Dethier, E. N., Renshaw, C. E., & Magilligan, F. J. (2022). Rapid changes to global river suspended sediment flux by humans. *Science*, 376(6600), 1447–1452. <https://doi.org/10.1126/science.abn7980>
- Donovan, M., Belmont, P., & Sylvester, Z. (2021). Evaluating the relationship between meander-bend curvature, sediment supply, and migration rates. *Journal of Geophysical Research: Earth Surface*, 126(3), e2020JF006058. <https://doi.org/10.1029/2020jfo06058>
- Edmonds, D. A., Martin, H. K., Valenza, J. M., Henson, R., Weissmann, G. S., Miltenberger, K., et al. (2022). Rivers in reverse: Upstream-migrating dechannelization and flooding cause avulsions on fluvial fans. *Geology*, 50(1), 37–41. <https://doi.org/10.1130/G49318.1>
- Fuller, I. C. (2008). Geomorphic impacts of a 100-year flood: Kivitea stream, Manawatu catchment, New Zealand. *Geomorphology*, 98(1–2), 84–95. <https://doi.org/10.1016/j.geomorph.2007.02.026>
- Gibson, S., & Shelley, J. (2020). Flood disturbance, recovery, and inter-flood incision on a large sand-bed river. *Geomorphology*, 351, 106973. <https://doi.org/10.1016/j.geomorph.2019.106973>
- Gintz, D., Hassan, M. A., & Schmidt, K.-H. (1996). Frequency and magnitude of bedload transport in a mountain river. *Earth Surface Processes and Landforms*, 21(5), 433–445. [https://doi.org/10.1002/\(sici\)1096-9837\(199605\)21:5<433::aid-esp580>3.0.co;2-p](https://doi.org/10.1002/(sici)1096-9837(199605)21:5<433::aid-esp580>3.0.co;2-p)
- Grill, G., Lehner, B., Thieme, M., Geenen, B., Tickner, D., Antonelli, F., et al. (2019). Mapping the world's free-flowing rivers. *Nature*, 569(7755), 215–221. <https://doi.org/10.1038/s41586-019-1111-9>
- Guzzetti, F., Ardizzone, F., Cardinali, M., Rossi, M., & Valigi, D. (2009). Landslide volumes and landslide mobilization rates in Umbria, central Italy. *Earth and Planetary Science Letters*, 279(3–4), 222–229. <https://doi.org/10.1016/j.epsl.2009.01.005>
- Hajdukiewicz, H., Wyżga, B., Mikuś, P., Zawiejska, J., & Radecki-Pawlik, A. (2016). Impact of a large flood on mountain river habitats, channel morphology, and valley infrastructure. *Geomorphology*, 272, 55–67. <https://doi.org/10.1016/j.geomorph.2015.09.003>
- Higgins, A., Restrepo, J. C., Ortiz, J. C., Pierini, J., & Otero, L. (2016). Suspended sediment transport in the Magdalena River (Colombia, South America): Hydrologic regime, rating parameters and effective discharge variability. *International Journal of Sediment Research*, 31(1), 25–35. <https://doi.org/10.1016/j.ijsrc.2015.04.003>

- Hofmeister, F., Arias-Rodriguez, L. F., Premier, V., Marin, C., Notarnicola, C., Disse, M., & Chiogna, G. (2022). Intercomparison of Sentinel-2 and modelled snow cover maps in a high-elevation Alpine catchment. *Journal of Hydrology X*, 15, 100123. <https://doi.org/10.1016/j.hydroa.2022.100123>
- Hooke, J. (2015). Variations in flood magnitude–effect relations and the implications for flood risk assessment and river management. *Geomorphology*, 251, 91–107. <https://doi.org/10.1016/j.geomorph.2015.05.014>
- Hooke, J. (2016). Geomorphological impacts of an extreme flood in SE Spain. *Geomorphology*, 263, 19–38. <https://doi.org/10.1016/j.geomorph.2016.03.021>
- Huang, C., Chen, Y., Zhang, S., & Wu, J. (2018). Detecting, extracting, and monitoring surface water from space using optical sensors: A review. *Reviews of Geophysics*, 56(2), 333–360. <https://doi.org/10.1029/2018rg000598>
- Huete, A., Didan, K., Miura, T., Rodriguez, E. P., Gao, X., & Ferreira, L. G. (2002). Overview of the radiometric and biophysical performance of the MODIS vegetation indices. *Remote sensing of environment*, 83(1–2), 195–213. [https://doi.org/10.1016/s0034-4257\(02\)00096-2](https://doi.org/10.1016/s0034-4257(02)00096-2)
- Isikdogan, L. F., Bovik, A., & Passalacqua, P. (2019). Seeing through the clouds with deepwatermap. *IEEE Geoscience and Remote Sensing Letters*, 17(10), 1662–1666. <https://doi.org/10.1109/lgrs.2019.2953261>
- Jarriel, T., Swartz, J., & Passalacqua, P. (2021). Global rates and patterns of channel migration in river deltas. *Proceedings of the National Academy of Sciences of the United States of America*, 118(46), e2103178118. <https://doi.org/10.1073/pnas.2103178118>
- Johnson, P. A., Hey, R. D., Horst, M. W., & Hess, A. J. (2001). Aggradation at bridges. *Journal of Hydraulic Engineering*, 127(2), 154–157. [https://doi.org/10.1061/\(asce\)0733-9429\(2001\)127:2\(154\)](https://doi.org/10.1061/(asce)0733-9429(2001)127:2(154))
- Kale, V. S. (2002). Fluvial geomorphology of Indian rivers: An overview. *Progress in Physical Geography*, 26(3), 400–433. <https://doi.org/10.1191/0309133302pp343ra>
- Kale, V. S. (2003). Geomorphic effects of monsoon floods on Indian rivers. In M. M. Q. Mirza, A. Dixit, & A. Nishat (Eds.), *Flood problem and management in South Asia* (pp. 65–84). Springer Netherlands. [https://doi.org/10.1007/978-94-017-0137-2\\_3](https://doi.org/10.1007/978-94-017-0137-2_3)
- Kale, V. S., & Hire, P. S. (2007). Temporal variations in the specific stream power and total energy expenditure of a monsoonal river: The Tapi River, India. *Geomorphology*, 92(3–4), 134–146. <https://doi.org/10.1016/j.geomorph.2006.06.047>
- Klingler, C., Schulz, K., & Herrnegger, M. (2021). LamaH-CE: LArge-SaMple DAta for hydrology and environmental sciences for central Europe. *Earth System Science Data*, 13(9), 4529–4565. <https://doi.org/10.5194/essd-13-4529-2021>
- Langhorst, T., & Pavelsky, T. (2022). Global observations of riverbank erosion and accretion from Landsat imagery. *Journal of Geophysical Research: Earth Surface*, 128(2), e2022JF006774. <https://doi.org/10.1029/2022JF006774>
- Larsen, I. J., Montgomery, D. R., & Korup, O. (2010). Landslide erosion controlled by hillslope material. *Nature Geoscience*, 3(4), 247–251. <https://doi.org/10.1038/ngeo776>
- Leenman, A., Eaton, B., & MacKenzie, L. G. (2022). Floods on alluvial fans: Implications for reworking rates, morphology and fan hazards. *Journal of Geophysical Research: Earth Surface*, 127(2), e2021JF006367. <https://doi.org/10.1029/2021jfo06367>
- Lehner, B., Verdin, K., & Jarvis, A. (2008). New global hydrography derived from spaceborne elevation data. *Eos, Transactions American Geophysical Union*, 89(10), 93–94. <https://doi.org/10.1029/2008eo100001>
- Liaw, A., & Wiener, M. (2002). Classification and regression by randomForest [Computer software]. *R News*, 2(3), 18–22. Retrieved from <https://CRAN.R-project.org/doc/Rnews/>
- Lindsay, J. B., & Ashmore, P. E. (2002). The effects of survey frequency on estimates of scour and fill in a braided river model. *Earth Surface Processes and Landforms: The Journal of the British Geomorphological Research Group*, 27(1), 27–43. <https://doi.org/10.1002/esp.282>
- Linke, S., Lehner, B., Dallaire, C. O., Ariwi, J., Grill, G., Anand, M., et al. (2019). Global hydro-environmental sub-basin and river reach characteristics at high spatial resolution. *Scientific Data*, 6(1), 283. <https://doi.org/10.1038/s41597-019-0300-6>
- Magilligan, F. J., Buraas, E., & Renshaw, C. (2015). The efficacy of stream power and flow duration on geomorphic responses to catastrophic flooding. *Geomorphology*, 228, 175–188. <https://doi.org/10.1016/j.geomorph.2014.08.016>
- Magilligan, F. J., Phillips, J. D., James, L. A., & Gomez, B. (1998). Geomorphic and sedimentological controls on the effectiveness of an extreme flood. *The Journal of Geology*, 106(1), 87–96. <https://doi.org/10.1086/516009>
- Marren, P. M. (2005). Magnitude and frequency in proglacial rivers: A geomorphological and sedimentological perspective. *Earth-Science Reviews*, 70(3–4), 203–251. <https://doi.org/10.1016/j.earscirev.2004.12.002>
- Martínez Silva, P., & Nanny, M. A. (2020). Impact of microplastic fibers from the degradation of nonwoven synthetic textiles to the Magdalena River water column and river sediments by the City of Neiva, Huila (Colombia). *Water*, 12(4), 1210. <https://doi.org/10.3390/w12041210>
- Messenger, M. L., Lehner, B., Grill, G., Nedeva, I., & Schmitt, O. (2016). Estimating the volume and age of water stored in global lakes using a geo-statistical approach. *Nature Communications*, 7(1), 1–11. <https://doi.org/10.1038/ncomms13603>
- Middleton, L., Ashmore, P., Leduc, P., & Sjogren, D. (2019). Rates of planimetric change in a proglacial gravel-bed braided river: Field measurement and physical modelling. *Earth Surface Processes and Landforms*, 44(3), 752–765. <https://doi.org/10.1002/esp.4528>
- Miller, A. J. (1990). Flood hydrology and geomorphic effectiveness in the central Appalachians. *Earth Surface Processes and Landforms*, 15(2), 119–134. <https://doi.org/10.1002/esp.3290150203>
- Morche, D., Schmidt, K.-H., Heckmann, T., & Haas, F. (2007). Hydrology and geomorphic effects of a high-magnitude flood in an alpine river. *Geografiska Annaler - Series A: Physical Geography*, 89(1), 5–19. <https://doi.org/10.1111/j.1468-0459.2007.00304.x>
- Nagel, G. W., de Moraes Novo, E. M. L., Martins, V. S., Campos-Silva, J. V., Barbosa, C. C. F., & Bonnet, M. P. (2022). Impacts of meander migration on the Amazon riverine communities using Landsat time series and cloud computing. *Science of the Total Environment*, 806, 150449. <https://doi.org/10.1016/j.scitotenv.2021.150449>
- Nanson, G. C., & Hickin, E. J. (1986). A statistical analysis of bank erosion and channel migration in western Canada. *Geological Society of America Bulletin*, 97(4), 497–504. [https://doi.org/10.1130/0016-7606\(1986\)97<497:asaobe>2.0.co;2](https://doi.org/10.1130/0016-7606(1986)97<497:asaobe>2.0.co;2)
- Pekel, J.-F., Cottam, A., Gorelick, N., & Belward, A. S. (2016). High-resolution mapping of global surface water and its long-term changes. *Nature*, 540(7633), 418–422. <https://doi.org/10.1038/nature20584>
- Pfeiffer, A. M., Collins, B. D., Anderson, S. W., Montgomery, D. R., & Istanbuluoglu, E. (2019). River bed elevation variability reflects sediment supply, rather than peak flows, in the uplands of Washington State. *Water Resources Research*, 55(8), 6795–6810. <https://doi.org/10.1029/2019wr025394>
- Pickens, A. H., Hansen, M. C., Hancher, M., Stehman, S. V., Tyukavina, A., Potapov, P., et al. (2020). Mapping and sampling to characterize global inland water dynamics from 1999 to 2018 with full Landsat time-series. *Remote Sensing of Environment*, 243, 111792. <https://doi.org/10.1016/j.rse.2020.111792>
- Restrepo, J. D., Kjerfve, B., Hermelin, M., & Restrepo, J. C. (2006). Factors controlling sediment yield in a major South American drainage basin: The Magdalena river, Colombia. *Journal of Hydrology*, 316(1–4), 213–232. <https://doi.org/10.1016/j.jhydrol.2005.05.002>
- Rose, T., Erskine, W., & Miners, B. (2020). A customised approach to determining the geomorphic effectiveness of small flood events in a regulated river. *River Research and Applications*, 36(4), 580–594. <https://doi.org/10.1002/rra.3498>

- Rousel, J., Haas, R., Schell, J., & Deering, D. (1973). Monitoring vegetation systems in the great plains with ERTS. In *Proceedings of the third Earth Resources technology Satellite—1 Symposium* (pp. 309–317). NASA SP-351.
- Rowland, J. C., Shelef, E., Pope, P. A., Muss, J., Gangodagamage, C., Brumby, S. P., & Wilson, C. J. (2016). A morphology independent methodology for quantifying planview river change and characteristics from remotely sensed imagery. *Remote Sensing of Environment*, 184, 212–228. <https://doi.org/10.1016/j.rse.2016.07.005>
- Schwenk, J., Khandelwal, A., Fratkin, M., Kumar, V., & Fofoula-Georgiou, E. (2017). High spatiotemporal resolution of river planform dynamics from Landsat: The RivMAP toolbox and results from the Ucayali River. *Earth and Space Science*, 4(2), 46–75. <https://doi.org/10.1002/2016ea000196>
- Slater, L. J. (2016). To what extent have changes in channel capacity contributed to flood hazard trends in England and Wales? *Earth Surface Processes and Landforms*, 41(8), 1115–1128. <https://doi.org/10.1002/esp.3927>
- Slater, L. J., Anderson, B., Buechel, M., Dadson, S., Han, S., Harrigan, S., et al. (2021). Nonstationary weather and water extremes: A review of methods for their detection, attribution, and management. *Hydrology and Earth System Sciences*, 25(7), 3897–3935. <https://doi.org/10.5194/hess-25-3897-2021>
- Slater, L. J., Singer, M. B., & Kirchner, J. W. (2015). Hydrologic versus geomorphic drivers of trends in flood hazard. *Geophysical Research Letters*, 42(2), 370–376. <https://doi.org/10.1002/2014GL062482>
- Smith, D. G. (1986). Anastomosing river deposits, sedimentation rates and basin subsidence, Magdalena River, northwestern Colombia, South America. *Sedimentary Geology*, 46(3–4), 177–196. [https://doi.org/10.1016/0037-0738\(86\)90058-8](https://doi.org/10.1016/0037-0738(86)90058-8)
- Surian, N., Barban, M., Ziliani, L., Monegato, G., Bertoldi, W., & Comiti, F. (2015). Vegetation turnover in a braided river: Frequency and effectiveness of floods of different magnitude. *Earth Surface Processes and Landforms*, 40(4), 542–558. <https://doi.org/10.1002/esp.3660>
- Sylvester, Z., Durkin, P., & Covault, J. A. (2019). High curvatures drive river meandering. *Geology*, 47(3), 263–266. <https://doi.org/10.1130/g45608.1>
- Tunncliffe, J., Brierley, G., Fuller, I. C., Leenman, A., Marden, M., & Peacock, D. (2018). Reaction and relaxation in a coarse-grained fluvial system following catchment-wide disturbance. *Geomorphology*, 307, 50–64. <https://doi.org/10.1016/j.geomorph.2017.11.006>
- Valenza, J., Edmonds, D., Hwang, T., & Roy, S. (2020). Downstream changes in river avulsion style are related to channel morphology. *Nature Communications*, 11(1), 1–8. <https://doi.org/10.1038/s41467-020-15859-9>
- Wasko, C., & Guo, D. (2022). Understanding event runoff coefficient variability across Australia using the hydroEvents R package [Computer software]. *Hydrological Processes*, 36(4), e14563. <https://doi.org/10.1002/hyp.14563>
- Webb, B., & Walling, D. (1982). The magnitude and frequency characteristics of fluvial transport in a Devon drainage basin and some geomorphological implications. *Catena*, 9(1–2), 9–23. [https://doi.org/10.1016/s0341-8162\(82\)80002-7](https://doi.org/10.1016/s0341-8162(82)80002-7)
- Wickert, A. D., Martin, J. M., Tal, M., Kim, W., Sheets, B., & Paola, C. (2013). River channel lateral mobility: Metrics, time scales, and controls. *Journal of Geophysical Research: Earth Surface*, 118(2), 396–412. <https://doi.org/10.1029/2012j002386>
- Wolman, M. G., & Gerson, R. (1978). Relative scales of time and effectiveness of climate in watershed geomorphology. *Earth Surface Processes*, 3(2), 189–208. <https://doi.org/10.1002/esp.3290030207>
- Wolman, M. G., & Miller, J. P. (1960). Magnitude and frequency of forces in geomorphic processes. *The Journal of Geology*, 68(1), 54–74. <https://doi.org/10.1086/626637>
- Xu, H. (2006). Modification of normalised difference water index (NDWI) to enhance open water features in remotely sensed imagery. *International Journal of Remote Sensing*, 27(14), 3025–3033. <https://doi.org/10.1080/01431160600589179>
- Yamazaki, D., Ikeshima, D., Tawatari, R., Yamaguchi, T., O'Loughlin, F., Neal, J. C., et al. (2017). A high-accuracy map of global terrain elevations. *Geophysical Research Letters*, 44(11), 5844–5853. <https://doi.org/10.1002/2017gl072874>
- Yousefi, S., Mirzaee, S., Keesstra, S., Surian, N., Pourghasemi, H. R., Zakizadeh, H. R., & Tabibian, S. (2018). Effects of an extreme flood on river morphology (case study: Karoon River, Iran). *Geomorphology*, 304, 30–39. <https://doi.org/10.1016/j.geomorph.2017.12.034>
- Zou, Z., Xiao, X., Dong, J., Qin, Y., Doughty, R. B., Menarguez, M. A., et al. (2018). Divergent trends of open-surface water body area in the contiguous United States from 1984 to 2016. *Proceedings of the National Academy of Sciences of the United States of America*, 115(15), 3810–3815. <https://doi.org/10.1073/pnas.1719275115>

## References From the Supporting Information

- Biedenharn, D. S., & Thorne, C. R. (1994). Magnitude-frequency analysis of sediment transport in the lower Mississippi river. *Regulated Rivers: Research & Management*, 9(4), 237–251. <https://doi.org/10.1002/rrr.3450090405>
- Breiman, L. (2001). Random forests. *Machine Learning*, 45(1), 5–32. <https://doi.org/10.1023/a:1010933404324>
- Church, M. (2010). Gravel-bed rivers. In T. Burt & R. Allison (Eds.), *Sediment cascades: An integrated approach* (pp. 241–269). Wiley-Blackwell.
- Lenzi, M., Mao, L., & Comiti, F. (2004). Magnitude-frequency analysis of bed load data in an Alpine boulder bed stream. *Water Resources Research*, 40(7), W07201. <https://doi.org/10.1029/2003wr002961>
- Rhoads, B. L. (1990). Hydrologic characteristics of a small desert mountain stream: Implications for short-term magnitude and frequency of bedload transport. *Journal of Arid Environments*, 18(2), 151–163. [https://doi.org/10.1016/s0140-1963\(18\)30849-8](https://doi.org/10.1016/s0140-1963(18)30849-8)
- Torizzo, M., & Pitlick, J. (2004). Magnitude-frequency of bed load transport in mountain streams in Colorado. *Journal of Hydrology*, 290(1–2), 137–151. <https://doi.org/10.1016/j.jhydrol.2003.12.001>
- Whittingham, M. J., Stephens, P. A., Bradbury, R. B., & Freckleton, R. P. (2006). Why do we still use stepwise modelling in ecology and behaviour? *Journal of Animal Ecology*, 75(5), 1182–1189. <https://doi.org/10.1111/j.1365-2656.2006.01141.x>